Available online at www.sciencedirect.com
SCIENCE DIRECT®
Optics Communications 255 (2005) 57–64
OPTICS COMMUNICATIONS
www.elsevier.com/locate/optcom

Secondary modulation instability in partially coherent beams

Björn Gütlich [a,*], Thomas König [a], Cornelia Denz [a], Kristian Motzek [b], Friedemann Kaiser [b]

[a] Institute of Applied Physics, University of Münster, Corrensstrasse 2-4, 48151 Münster, Germany
[b] Institute of Applied Physics, Darmstadt University of Technology, Hochschulstrasse 4a, 64289 Darmstadt, Germany

Received 3 February 2005; received in revised form 26 April 2005; accepted 31 May 2005

Abstract

Due to modulation instability partially incoherent optical beams break up into stripe filaments in noninstantaneous media at a first threshold. We numerically and experimentally report on the formation of two-dimensional filaments at a secondary threshold, if increasing the nonlinearity further, which is due to material anisotropy. Particularly, we investigate the dependence of this secondary modulation instability on the coherence properties of the beam, using a photorefractive nonlinearity. From the measurement of modulation contrast in two dimensions and additionally using a Fourier method we quantitatively derive experimental thresholds for first and secondary onset of modulation instability and study how both onsets relate to the coherence properties of the beam.

PACS: 42.65.Tg; 42.65.Hw; 42.25.Kb

Keywords: Nonlinear optics; Modulation instability; Photorefractive crystal; Incoherent; Soliton

1. Introduction

Modulation instability (MI) is a very general phenomenon in nonlinear science [1]. In presence of a nonlinearity a noisy uniform solution becomes unstable against perturbations of a specific length or time scale. These specific perturbations become self-amplified and finally a self-organized solution with a scaling typical for the system evolves. Examples for such behaviour may be found in many fields and also play an important role in optics. In the context of optical systems at first regarded as a nuisance, later on the potential importance of these processes for the development of concepts in optical information processing have been recognized and consequently intensive

* Corresponding author. Tel.: +49 251 83 3351; fax: +49 251 8333513.
E-mail address: guetlich@uni-muenster.de (B. Gütlich).

0030-4018/$ - see front matter © 2005 Elsevier B.V. All rights reserved.
doi:10.1016/j.optcom.2005.05.053

research activity was triggered. Especially the formation of temporally and spatially localized structures such as solitons has attracted considerable attention for this reason [2,3]. A two-dimensional transversal modulation instability of the optical beam is to be considered as a crucial pre-condition for the existence of such spatial optical solitons, because a fundamental requirement for a spatial optical soliton, namely the balance between diffraction-induced beam broadening and a self-focussing nonlinearity, is found at the same parameter regions as MI. If MI is present, a broad optical beam will break up into small transversal filaments while propagating within a self-focussing nonlinear medium [4–8]. Assuming a spatially isotropic nonlinear response of the material, the filamentation transversal to the propagation direction, would also be expected to occur isotropically. However, in case of anisotropic media, such as photorefractive crystals, an anisotropic nonlinear response must be expected. And indeed, in photorefractive materials it is found that dependent on both the strength of the nonlinearity and the propagation distance the uniform beam first breaks up into (1 + 1) dimensional (D) stripes and only later on at either higher propagation distances or stronger nonlinearities (2 + 1)D beam filaments develop [5].

In principle one expects MI to occur only with coherent beams. If the nonlinear material however exhibits a noninstantaneous response, the observation of MI with incoherent beams is possible as long as the phase fluctuations of the beam are faster than the response time of the material [8–14]. MI of such partially incoherent beams has gained attraction, because a change in interaction characteristic of incoherent solitons has been observed and therefore the prospect for more closely packed arrays of non-interacting solitons is opened [15,16]. Up to now MI of incoherent beams has been mainly studied with an approach regarding (1 + 1)D solutions, which may be extended to (2 + 1)D structures if assuming a spatially isotropic material response [11]. As a first approach this approximation is sufficient to explain the major effects. The delayed onset of (2 + 1)D filamentation via (1 + 1)D stripe solution as it has been observed in the coherent case [5] cannot be covered if the material anisotropy is excluded. Although the behaviour of the in experiment most commonly used photorefractive nonlinearity is determined by anisotropy, up to now the threshold behaviour of MI in noninstantaneous media and partially incoherent beams has not yet been studied including anisotropy-induced phenomena. In our contribution we especially address the aspect of anisotropy induced phenomena of MI when using incoherent light and a photorefractive nonlinearity. Particularly, we are interested in the onset of the secondary (2 + 1)D MI in dependence on the beam's coherence properties, which cannot be covered in an isotropic approach. At first we will discuss MI of incoherent beams, using a numerical approach. Later on we present experimental results, which we analyse with different methods in respect to the onset of the secondary fully two-dimensional modulation instability.

2. Numerical model for incoherent modulation instability in anisotropic media

In order to numerically study modulation instability of incoherent beams we model the propagation of incoherent light in a photorefractive medium. The model explicitly includes the full characteristics of the photorefractive nonlinearity and particularly the anisotropic material response is covered.

A light beam propagating through a photorefractive medium in z-direction can be described in paraxial approximation by the equation

$$2ik_0 n_e \frac{\partial}{\partial z} A + \nabla_\perp^2 A = -k_0^2 n_e^4 r_{33} \frac{\partial \varphi}{\partial x} A, \qquad (1)$$

where $\nabla_\perp = \partial_x^2 + \partial_y^2$, k_0 is the vacuum wavenumber of the light beam, n_e is the refractive index of the (unperturbed) medium and r_{33} is the effective element of the electro-optical tensor. φ is the electric space charge potential inside the medium. For our simulations we used, in agreement with the experimental configuration, $k_0 = 2\pi/532$ nm, $n_e = 2.3$ and $r_{33} = 180$ pm/V. A is the envelope of the electric field of the light beam. In order to cover for the incoherence of the light beam, the coherent density model is used, which states that incoherent

light can be described as a superposition of many coherent, yet mutually incoherent components, propagating in slightly different directions. We thus express the light beam at the input face of the medium as:

$$A(x,y,0) = \sum_{k_x,k_y} P(x,y)\exp(\mathrm{i}(k_x x + k_y y))\frac{l_c}{\sqrt{\pi}} \times \sqrt{\exp(-(k_x^2+k_y^2)l_c^2/2)}\exp(\mathrm{i}\gamma_{k_x,k_y}(t)), \quad (2)$$

where $|P(x,y)|^2$ is the intensity profile of the beam at the input face, k_x and k_y stand for the slight tilting of the different components, l_c is the coherence length of the light and $\gamma_{k_x,k_y}(t)$ are random phase factors that are uncorrelated to each other, thus making the single components mutually incoherent. The factor $\exp(-(k_x^2+k_y^2)l_c^2/2)$ stands for a Gaussian distribution of the mutually incoherent k-vector components. We chose the maximum intensity of our incoherent beam to be around unity (measured in units or the dark intensity I_d). To excite the instability, we add around 1% of noise to the initial input beam.

Since plane waves with truly infinite spatial extent cannot be realized in numerical simulations, we chose to use a large grid and periodic boundary conditions to minimize the effects of the edges on the instability.

Photorefractive crystals are known to be well-described by the Kukhtarev equations, which yield, using a few well justified approximations, the following differential equation for the space charge potential [17]:

$$\nabla_\perp^2\varphi + \nabla_\perp \ln(1+I)\nabla_\perp\varphi = E_0\frac{\partial}{\partial x}\ln(1+I), \quad (3)$$

where E_0 is the external field applied parallel to the crystal's $\hat{c}$-axis (in the following we will choose $E_0 = 2.5$ kV/cm) and I is the intensity of the light beam, scaled to the dark intensity I_d, describing the excitation of charge carriers into the conduction band by thermal excitation or background illumination of the crystal. Remember that we are dealing with incoherent light. Hence, the intensity I is given by the sum of the intensities of the single components introduced in Eq. (2) and propagated using Eq. (1).

Fig. 1 shows the results of the numerical propagation of light with different degrees of coherence. Each column shows light with a different value of l_c. The leftmost column shows the fully coherent case, i.e., $l_c = \infty$, while for the other columns $l_c = 16$, 13 and 11 μm from left to right. The light beam is shown at the input face, after $z = 6$, 8, 10 and 12 mm of propagation. The pictures are oriented such that the $\hat{c}$-axis of the photorefractive crystal is horizontal. The pictures show that for all degrees of coherence, MI first breaks the plane wave into stripes oriented perpendicular to the $\hat{c}$-axis. In the coherent case, these stripes then break into filaments, as is known for quite a while [5]. If the degree of coherence of the light is decreased, however, the breaking of the stripes can be suppressed. For $l_c = 16$ μm one can see that extent of the filaments in the vertical direction is much longer than in the case of the fully coherent light. Decreasing of the degree of coherence further then leads to a complete stabilization of the stripes. Reducing the degree of coherence even further

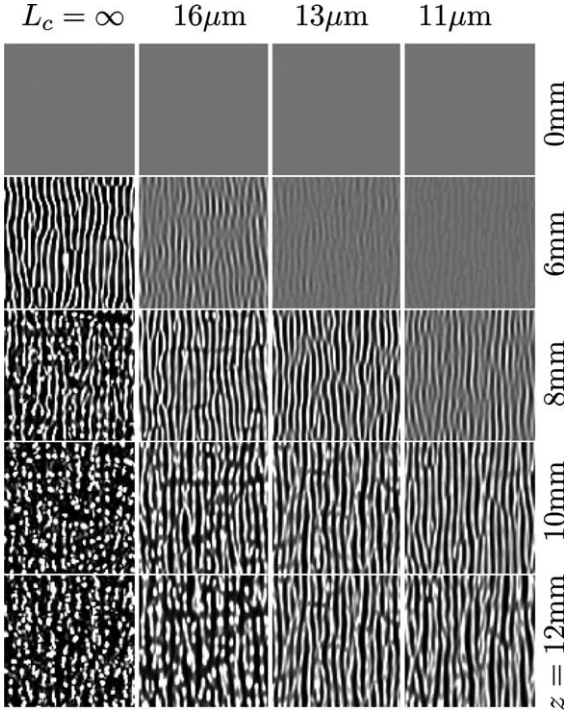

Fig. 1. Modulation instability in numerical simulations: rows depict equal propagation distance. Columns depict equal coherence properties.

would lead to a complete suppression of MI. The plane wave then would propagate through the medium without changing its shape.

3. Experimental observation of incoherent modulation instability in photorefractive crystals

The light source for our experiment is a Nd:YAG cw-laser at $\lambda = 532$ nm. To create a partially incoherent beam, a rotating diffuser is placed between two lenses in a 4f arrangement. The degree of spatial coherence is controlled with the diffuser position on the z-axis. According to the beam diameter at the diffuser the speckle size and thus the degree of spatial coherence length is modified. The collimated beam then propagates through a Cerium doped Strontium Barium Niobate crystal SBN:61 (5 mm × 5 mm × 23 mm, in width, height and length) to which an external electric field is applied along the crystal's $\hat{c}$-axis. The beam is extraordinarily polarized and thus experiences a nonlinear change of refractive index depending on the external field and on the total light intensity. The dark current density of the crystal is controlled with a white light background illumination. The intensity distribution at the crystal's backplane is recorded with a CCD-camera, while the input intensity is monitored with a photodiode. As an equivalent to the spatial coherence length l_c the average full half width of the speckles at the crystal's frontplane is taken, when the diffuser was stopped. It is made sure that the diffuser rotates much faster than the material's response time τ, which is in the order of a second for the crystal in use [18].

The intensity output was monitored at a fixed coherence length l_c, while the nonlinearity of the SBN crystal was increased by raising the externally applied voltage U_{ext} in increments of 100 V. For analysis, the images of the beam profile were recorded at every voltage step after approximately 2 min, permitting for transients to disappear. The applied external electric field was restricted to maximum values of 3 kV/cm to avoid damage of the crystal. Experiments were performed in the same manner for different coherence lengths varying between $l_c = 280$ and 9 μm. During all measurements input intensity ($I = 480$ μW/cm^2) as well as background illumination ($I_{\text{white light}} \approx 700$ μW/cm^2) were kept constant. Only approximate levels for the intensity of the background illumination at the crystal position can only be given due to the divergence and the spectral width of the white light. In Fig. 2, images of developing MI are shown. Rows depict system states at equal nonlinearity, while columns show pictures at equal coherence properties. At a fixed coherence length l_c (e.g., the $l_c = 280$ μm column) starting from a nearly uniform state the system develops first a stripe pattern, perpendicularly to the $\hat{c}$-axis, followed by the formation of spot like filaments at higher voltages. Small modulations found in the uniform state (0 V) most likely result from striations of the crystal and probably act as a trigger for the formation of stripes [14]. From the images it becomes also

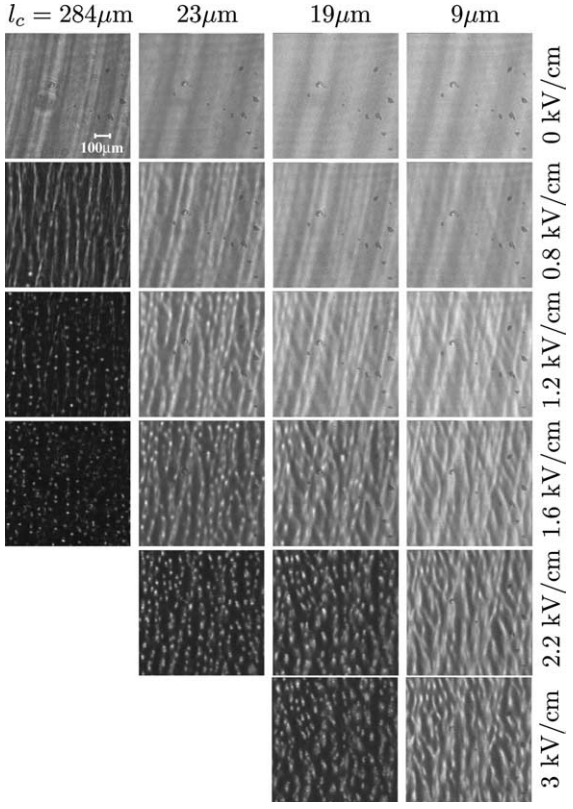

Fig. 2. Experimental images of modulation instability. Images in a row: the nonlinearity is equal. Images in a column: the degree of coherence is constant. With decreased coherence modulation instability sets in later.

obvious that as well formation of (1 + 1)D stripes as the decay of stripes in (2 + 1)D filaments occurs later, if the coherence length is decreased. Other groups observed tilting of the stripes up to an angle of 45° [11,12], in our experiment however only a very small tilt of approximately 1–5° compared to the initial striations in the crystal has been observed. The resulting (1 + 1)D MI stripes are in good approximation oriented perpendicularly to the crystal's $\hat{c}$-axis. At very small coherence lengths (e.g., 9 μm) (2 + 1)D MI is strongly suppressed and we observe zig-zag-kind of patterns instead of pronounced stripes. With decreasing coherence also the contrast of the pattern decreases.

4. Experimental thresholds for secondary modulation instability

To gain a quantitative measure for the experimental thresholds of MI the mean contrast $C(x_i)$ of image profiles has been determined along the images' horizontal x- and the vertical y-axis, respectively, with the following equation:

$$C(x_i) = \langle (I_{\max} - I_{\min})/(I_{\max} + I_{\min}) \rangle,$$

where x_i denotes either the x- or y-direction. We determined the mean contrast by first calculating the average contrast of a single image profile line. The total mean contrast $C(x_i)$ plotted over the external bias in Fig. 3 was derived from 600 lines. The curves in the graph are guides for the eye, which connect the measurement points at fixed coherence lengths l_c. The legend in the insertion of Fig. 3 denotes the coherence lengths at which measurements were performed. Fig. 3(a) shows the averaged contrast $C(x)$ (parallel to the crystal's $\hat{c}$-axis). Typically (e.g., at l_c = 284 μm (◇)) at first a rise in contrast is observed, which is generated by the formation of the (1 + 1)D stripe pattern. The rise is used to determine an experimental threshold for (1 + 1)D MI, as which we define the rise above the level of $(1 - 1/e)$ = 63% times the maximum of contrast (plotted as + in Fig. 7). As in our experiment the observed tilt angle between x-axis and stripe pattern is very small, this method to us seems justified. However for comparison later on also thresholds are derived from the angular modes in Fourier space are derived [13,14].

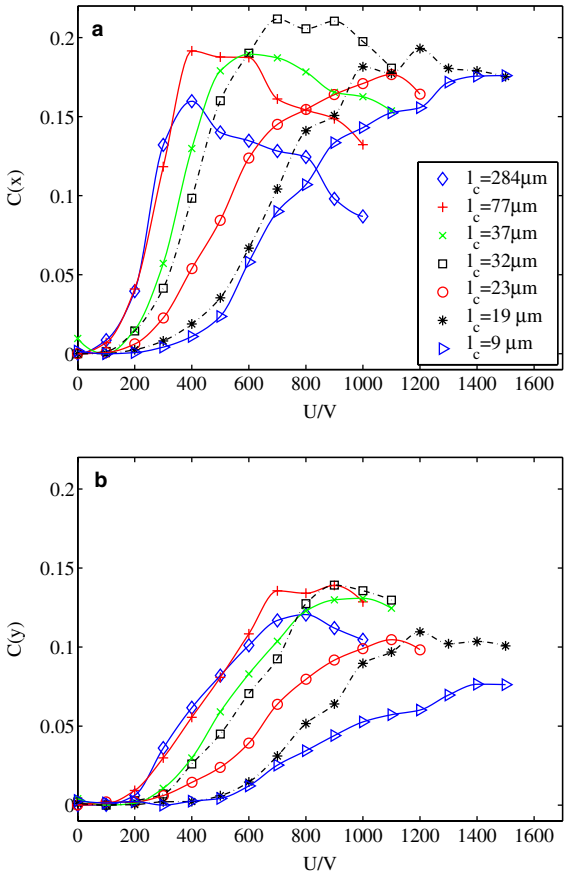

Fig. 3. (a) The averaged contrast of the images along the x direction $C(x)$ parallel to the $\hat{c}$-axis and (b) along the y-direction $C(y)$ over the applied voltage yield the dependence of the onset of MI on coherence length. From $C(x)$ and $C(y)$ experimental thresholds are derived. The legend applies to (a) and (b).

If only the first (1 + 1)D MI was involved one would expect the contrast $C(x)$ to remain at a constant saturation level, but typically the contrast decreases from its maximum value onwards (e.g., at 1 kV/cm at l_c = 284 μm). Note, that the decline in contrast is less pronounced for measurements at smaller coherence lengths l_c and also sets in later. In the case of coherence lengths of l_c = 19 and 9 μm even no significant decrease of the contrast is observed below 3 kV/cm. We conclude that the drop in contrast is caused by the onset of the secondary (2 + 1)D MI. Due to the break up of the stripe solution, now also the y-profiles become modulated, which reaffects $C(x)$. To check this assumption also the mean contrasts of the y-profiles

$C(y)$ are plotted in Fig. 3(b). Along the y-profiles the rise of contrast occurs at higher nonlinearities (e.g., at $l_c = 280$ μm the maximum of $C(y)$ is reached at 1.4 kV/cm, instead of at 0.8 kV/cm for $C(x)$.) We define an experimental threshold for (2 + 1)D MI as before as the rise above the level of $(1 - 1/e)$ times the maximum of $C(y)$ (* in Fig. 7). However, at the coherence lengths $l_c = 9$ and 19 μm $C(y)$ does not yet reach a well pronounced maximum below 3 kV/cm, therefore the (2 + 1)D thresholds for these coherence length are to be neglected. Comparison with images of MI at $l_c = 9$ μm (Fig. 2) indicates that at these low coherence length potentially the formation of (1 + 1) D MI is suppressed in favour of a kind of zig-zag pattern, shown in Fig. 2, which seems to smears out the contrast measurement.

Similar results can be obtained from the numerical simulations. The plots of the average contrasts $C(x)$ and $C(y)$ can be found in Fig. 4. Qualitatively good agreement in the progression of experimental- and numerical contrast functions is observed. Quantitatively however comparison to the experimental results is difficult because the propagation length was used as parameter in numerics, while in the experiments the nonlinearity of the material is varied. Note, that typically the threshold for the onset of nonlinear behaviour is derived theoretically using a more rigid stability analysis. Here, we therefore refrain from the determination of numerical thresholds and restrict ourselves to a qualitative comparison.

To validate our previous results we also derived experimental thresholds from a Fourier analysis of the light field, as also used by Chen et al. [13,14]. From the Fourier transform we calculate the angular distribution of spatial frequencies:

$$f(\theta_0) = \int_{\theta_0-\Delta\theta}^{\theta_0+\Delta\theta} \int_0^{k_{\max}} \mathrm{d}k\, \mathrm{d}\theta \mathscr{I}(k,\theta), \qquad (4)$$

where $\mathscr{I}(k,\theta) = \mathscr{F}\mathscr{T}(I(x,y))$ is the Fourier transform of the intensity distribution, and with $\Delta\theta = 1°$ and θ_0 varying from 0° to 360° in increments of 2°. In presence of the stripe (1 + 1)D MI perpendicularly to the stripe orientation pronounced peaks appear in the angular distribution $f(\theta)$, while as well without MI present as at fully developed (2 + 1)D MI, $f(\theta)$ shows no peaking (see

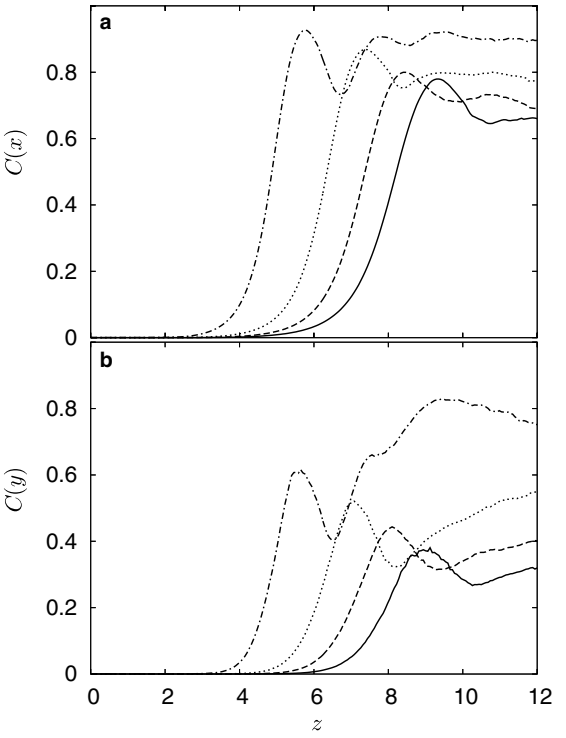

Fig. 4. Contrast functions $C(x)$ and $C(y)$ calculated from numerical simulations. (dash-dotted: coherent, dotted: l_c = 16 μm, dashed: l_c = 13 μm, solid line: l_c = 11 μm).

Fig. 5(a)). Thus, now we determined the averaged contrast $C(f(\theta)) = (\max\{f(\theta)\} - \max\{f(\theta)\})/(\max\{f(\theta)\} + \max\{f(\theta)\})$ of the angular distribution profiles, which is plotted in Fig. 5(b). From the contrasts we define experimental thresholds as follows: As the threshold of (1 + 1)D MI we take the rise above $1/e$*max($f(\theta)$) (□ in Fig. 7) and for the (2 + 1)D MI we define the descend below $(1 - 1/e)$*max($f(\theta)$) as threshold (○ in Fig. 7). As before similar results are obtained for the contrast function $C(f(\theta))$ derived with the Fourier method from numerical simulation as comparison with the plot in Fig. 6 shows.

In Fig. 7 experimental thresholds for (1 + 1)D (+, □) and (2 + 1)D MI (*, ○), defined above are plotted. Comparison of the thresholds derived from $C(x)$ and $C(y)$ with the ones derived from $C(f(\theta))$ shows that for (1 + 1)D MI the $C(f(\theta))$ thresholds (□) remain below the $C(x)$ thresholds (+), while the $C(f(\theta))$ (2 + 1)D MI thresholds (○) stay above the $C(y)$ thresholds (*). This differences are due to

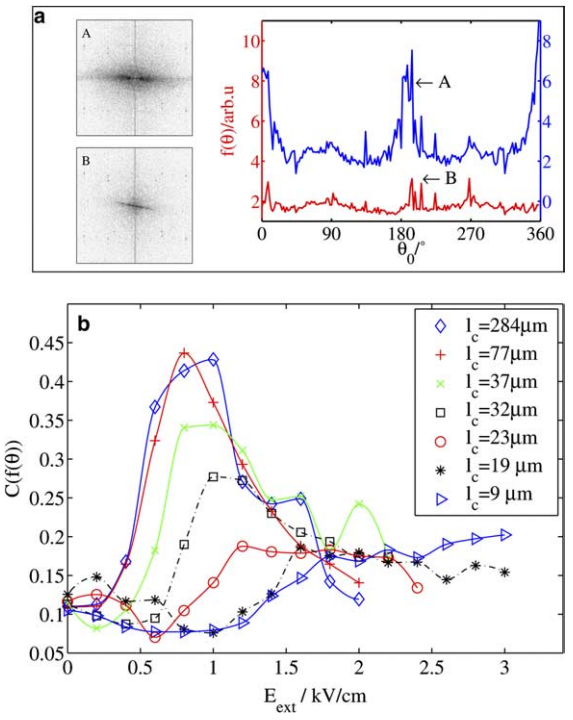

Fig. 5. (a) Fourier transform of the near field at l_c = 280 μm (A, 0.8 kV/cm; B, 0 V) and their corresponding angular distribution $f(\theta)$ of spatial frequencies. (b) Contrast $C(f(\theta))$ of the angular distributions. The lines in (b) are guides for the eye.

the choice of values for the definition of thresholds. Fine tuning of these values probably would gain better coincidence, but the difference can also be used as an estimation for the error bars of the measurement. The difference for the (2 + 1)D MI thresholds however becomes especially pronounced for very small coherence lengths. Here, the difference can be regarded as an indicator for the formation of the zig-zag like pattern. The onset of full filamentation is in this parameter region covered better by the Fourier method $C(f(\theta))$. Regarding the general progression of (1 + 1)D experimental thresholds in relation to (2 + 1)D MI thresholds at first these values do not change with decreased coherence length. In this parameter region also both threshold approximatively have a fixed ratio to each other, which can be viewed as indication for the anisotropy of the SBN crystal's nonlinear response. Only at a coherence length of approximately l_c = 45 μm both experimental thresholds start to alter and a steep increase of both is observed. Considering only the behaviour of the experimental thresholds of MI, the coherence length l_c = 45 μm can be interpreted as the nonlinear coherence length of MI. Up to this point the nonlinear response to the partially coherent beam is equivalent to the coherent behaviour, from then on the influences of incoherent fluctuations push the experimental thresholds for MI upwards and also the fixed relation between thresholds ceases to exist.

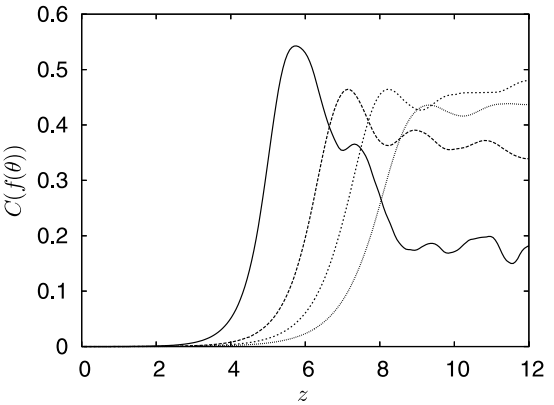

Fig. 6. Numerical results on the contrast $C(f(\theta))$ of the angular distributions.

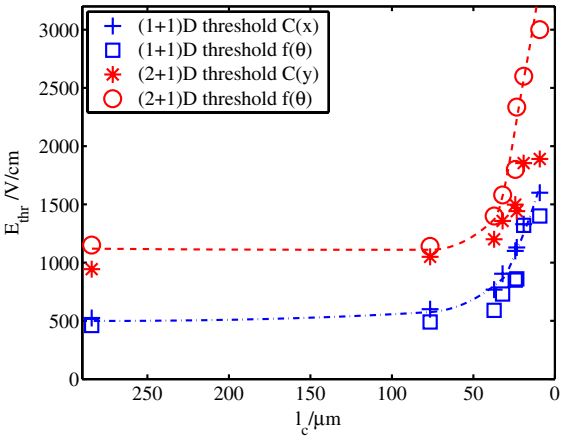

Fig. 7. Plot of first (1 + 1)D experimental threshold, derived from $C(x)$ (+) and from $C(f(\theta))$ (□), as well as secondary (2 + 1)D MI experimental threshold derived from $C(y)$ (∗) and from $C(f(\theta))$ (○) in dependence of the beam's coherence properties. The lines are guides to the eye.

5. Conclusion

We have presented experimental and numerical results on two-dimensional modulation instability of incoherent beams in anisotropic media. The onset of (1 + 1)D and (2 + 1)D MI was investigated experimentally and numerically in dependence of the spatial coherence length. At moderate incoherence the experimental thresholds of MI are not affected by alteration of coherence properties. If the beam becomes more strongly incoherent the experimental thresholds of MI increase steeply. At very low coherence lengths numerics and experiment indicates to the development of zig-zag kind of patterns in favour of (1 + 1)D filamentation, which was analysed by help of two different methods in determining experimental threshold of MI. A good qualitative agreement of numerical and experimental results can be stated.

References

[1] M.C. Cross, P.C. Hohenberg, Rev. Mod. Phys. 65 (3) (1993) 851.
[2] M. Segev, B. Crosignani, A. Yariv, B. Fischer, Phys. Rev. Lett. 68 (7) (1992) 923.
[3] J. Petter, J. Schröder, D. Träger, C. Denz, Opt. Lett. 28 (6) (2003) 438.
[4] V.I. Bespalov, V.I. Talanov, JETP Lett. USSR 3 (12) (1996) 307.
[5] A.V. Mamaev, M. Saffman, D.Z. Anderson, A.A. Zozulya, Phys. Rev. A 54 (1) (1996) 870.
[6] A.V. Mamaev, M. Saffman, A.A. Zozulya, Europhys. Lett. 35 (1) (1996) 25.
[7] M. Peccianti, C. Conti, G. Assanto, Phys. Rev. E 68 (2003) R025602.
[8] J. Klinger, H. Martin, Z. Chen, Opt. Lett. 26 (5) (2001) 271.
[9] M. Soljacic, M. Segev, T. Coskun, D.N. Christodoulides, A. Vishwanath, Phys. Rev. Lett. 84 (2000) 467.
[10] S.M. Sears, M. Soljacic, D.N. Christodoulides, M. Segev, Phys. Rev. E 65 (2002) 036620.
[11] D. Kip, M. Soljacic, M. Segev, S.M. Sears, D.N. Christodoulides, J. Opt. Soc. Am. B 19 (3) (2002) 502.
[12] D. Kip, M. Soljacic, M. Segev, E. Eugenieva, D.N. Christodoulides, Science 290 (2000) 495.
[13] Z. Chen, J. Klinger, D.N. Christodoulides, Phys. Rev. E 66 (2002) 066601.
[14] Z. Chen, S.M. Sears, H. Martin, D.N. Christodoulides, M. Segev, Proc. Nat. Acad. Sci. 99 (2002) 5223.
[15] W. Krolikowski, B. Luther-Davies, C. Denz, J. Petter, C. Weilnau, A. Stepken, M. Belic, Appl. Phys. B 68 (5) (1999) 975.
[16] C. Weilnau, C. Denz, J. Opt. A Pure Appl. Opt. 5 (2003) 529.
[17] A.A. Zozulya, D.Z. Anderson, Phys. Rev. A 51 (2) (1995) 1520.
[18] K. Buse, A. Gerwens, S. Wevering, E. Krätzig, Josa B 15 (6) (1998) 1674.